Chemical Engineering Science, Vol. 44, No. 10, pp. 2333–2344, 1989.
Printed in Great Britain.

0009-2509/89 $3.00 + 0.00

MODELING ADSORPTION IN LIQUID–SOLID FLUIDIZED BEDS

S. VEERARAGHAVAN and L. T. FAN†
Department of Chemical Engineering

and

A. P. MATHEWS
Department of Civil Engineering, Kansas State University, Manhattan, KS 66506, U.S.A.

(*Received* 14 *July* 1988; *accepted* 25 *January* 1989)

Abstract—Under certain conditions, the breakthrough time in a fluidized-bed adsorber is considerably shorter than that in a comparable fixed-bed adsorber. This phenomenon is probably due to the appreciable macroscale or axial mixing occurring in the solid and liquid phases of the fluidized bed. An axial dispersion model has been adapted to characterize the fluidized-bed adsorber. The model takes into account the effects of axial mixing in the solid and liquid phases, mass transfer resistance in the laminar fluid boundary surrounding an individual adsorbent particle, and diffusional resistance within the particle. The model has been solved numerically to simulate the performance of a laboratory-scale adsorber. The results of the simulation closely represent experimental observations over wide ranges of the influent flow rate, fluidized-bed height and adsorbent particle size.

INTRODUCTION

Adsorption with activated carbon is widely employed for the removal of organics in water purification. Several adsorber configurations are possible for treatment with activated carbon; these include batch vessel, continuous flow stirred tank, fixed bed, moving bed, and fluidized bed [e.g. Culp *et al.* (1978)]. Traditionally, the treatment of choice has been packed-bed adsorption due to the ease and reliability of this operation. Nevertheless, several problems, such as excessive head loss, air binding, and fouling with biological and particulate matter are associated with packed-bed operation. These problems are significantly reduced in fluidized-bed adsorption; hence, our research recently has focused on this mode of operation.

The breakthrough time in a fluidized-bed adsorber is, however, considerably shorter than in an adsorber operating at comparable conditions but whose bed is prevented from expanding by a restricting device (Mathews and Fan, 1983). This is probably due to the substantial macroscale or axial mixing occurring in both the solid and liquid phases of the fluidized bed. In the present work, an axial dispersion model has been adapted to represent the system.

MODEL DEVELOPMENT

The governing equations of the present model have been derived based on several simplifying assumptions. These assumptions and derivation of the equations are given in this section.

Assumptions

The governing equations of the model have been derived based on the following suppositions.

(1) The granular activated carbon (hereafter refered to as GAC) is of uniform particle size. This condition can be closely approximated in laboratory experiments by choosing GAC particles with a narrow mesh size range. The particles are also assumed to be spherical in shape.
(2) The cross-sectional area of the adsorber is constant.
(3) The radial concentration gradients are negligible in both the liquid and solid phases of the adsorber.
(4) The adsorption process is sufficiently rapid so that a local equilibrium is established at the particle surface between the phenol concentrations in the solution and the adsorbed phase. This is usually the case in activated carbon adsorption [e.g. Ruthven (1984)].
(5) The rate of adsorption is limited by the intraparticle diffusional resistance and the mass transfer resistance in the laminar fluid boundary layer surrounding an individual adsorbent particle.
(6) The transfer of adsorbate into the particle can be described by the homogeneous solid diffusion model [e.g. Suzuki and Kawazoe (1975)].
(7) Thermal effects are negligible, i.e. the adsorber operates isothermally.
(8) The hydrodynamic behavior of the GAC particles and the fluidizing liquid in the adsorber can be described by the axial dispersion model. It has been shown [e.g. Carlos and Richardson (1968), Chung and Wen (1968), and Van Der Meer *et al.* (1984)] that the motion of particles and fluid

†Author to whom correspondence should be addressed.

elements in a liquid–solid fluidized bed can be appropriately described by means of an axial dispersion-type continuum model.

Derivation of the governing equations

In writing the material balance equations for the adsorbate, we need to resolve the difficulty involved in describing the system consisting of finite-sized GAC particles as a continuum. This has been accomplished by writing the material balance equations for the adsorber in two stages.

Stage 1. In stage 1, GAC particles are treated as a continuous solid phase. A schematic representation of the system is shown in Fig. 1. At this level, a GAC particle is envisioned as a point particle with its adsorbate concentration equal to the volume average concentration over the particle. The degree of axial mixing of the fluidizing liquid and that of fluidized particles in a liquid–solid fluidized bed are expressed in terms of the dispersion coefficients (Chung and Wen, 1968; Potter, 1971; Van Der Meer *et al.*, 1984); the so-called closed boundary conditions, arising from the continuity conditions, are assumed at the inlet and outlet of the adsorber for both the liquid and solid phases.

The mass balance with respect to the adsorbate around the liquid phase between heights z and $z+\Delta z$ gives

$$\begin{bmatrix}\text{accumulation}\\ \text{rate}\end{bmatrix}=\begin{bmatrix}\text{in by}\\ \text{dispersion}\end{bmatrix}-\begin{bmatrix}\text{out by}\\ \text{dispersion}\end{bmatrix}+\begin{bmatrix}\text{in by}\\ \text{convection}\end{bmatrix}-\begin{bmatrix}\text{out by}\\ \text{convection}\end{bmatrix}-[\text{loss by adsorption}]$$

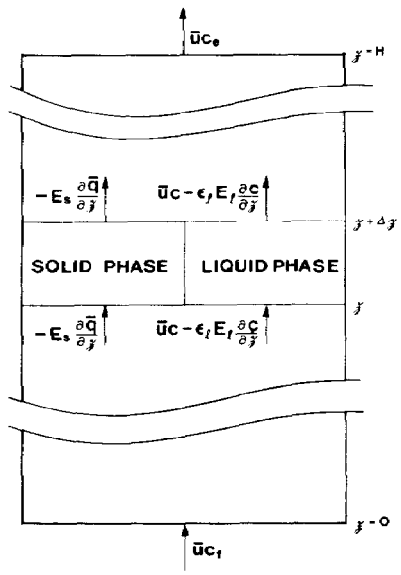

Fig. 1. Schematic representation of the fluidized-bed adsorber.

i.e.

$$\varepsilon_l\frac{\partial C}{\partial t}=E_l\varepsilon_l\frac{\partial^2 C}{\partial z^2}-\bar{u}\frac{\partial C}{\partial z}-\frac{3k_f\varepsilon_s(C-C^*)}{R}. \tag{1}$$

The initial and boundary conditions are

$$t=0,\quad C(z,0)=C_z(0),\qquad 0\leqslant z\leqslant H \tag{1a}$$

$$z=0,\quad C-\frac{E_l\varepsilon_l}{\bar{u}}\frac{\partial C}{\partial z}=C_f,\quad t>0 \tag{1b}$$

$$z=H,\quad \frac{\partial C}{\partial z}=0,\quad t>0. \tag{1c}$$

There is no convective flow in the solid phase; hence,

$$\begin{bmatrix}\text{accumulation}\\ \text{rate}\end{bmatrix}=\begin{bmatrix}\text{in by}\\ \text{dispersion}\end{bmatrix}-\begin{bmatrix}\text{out by}\\ \text{dispersion}\end{bmatrix}+[\text{gain by adsorption}]$$

i.e.

$$\varepsilon_s\frac{\partial\bar{q}}{\partial t}=E_s\frac{\partial^2\bar{q}}{\partial z^2}+\frac{3k_f\varepsilon_s(C-C^*)}{\rho_p R}. \tag{2}$$

The initial and boundary conditions are

$$t=0,\quad \bar{q}(z,0)=\bar{q}_z(0),\quad 0\leqslant z\leqslant H \tag{2a}$$

$$z=0,\quad \frac{\partial\bar{q}}{\partial z}=0,\qquad t>0 \tag{2b}$$

$$z=H,\quad \frac{\partial\bar{q}}{\partial z}=0,\qquad t>0. \tag{2c}$$

Stage 2. In the second stage, the mass balance equations are derived for a finite-sized GAC particle at axial position z. On applying the homogeneous solid diffusion model [e.g. Suzuki *et al.* (1974)] to a single particle at position z, we obtain

$$\frac{\partial q_z(r,t)}{\partial t}=\left(\frac{D_e}{r^2}\right)\frac{\partial}{\partial r}\left(r^2\frac{\partial q_z}{\partial r}\right),\quad 0\leqslant z\leqslant H. \tag{3}$$

The initial and boundary conditions are

$$t=0,\quad q_z(r,0)=q(z,r,0),\quad 0\leqslant z\leqslant H \tag{3a}$$

$$r=0,\quad \frac{\partial q_z}{\partial r}=0,\qquad t>0 \tag{3b}$$

$$r=R,\quad \frac{\partial q_z}{\partial r}=\frac{R}{3D_e}\frac{\partial\bar{q}_z}{\partial t},\qquad t>0. \tag{3c}$$

Note that the boundary condition (3c) at GAC particle surface is written in terms of the rate of change of the volume average concentration $\partial\bar{q}_z/\partial t$, obtained from eq. (2) for a particle at position z. This equation includes the terms for intermixing of the particles and the terms for adsorbate gain due to the mass transfer from the liquid phase.

Finally, we need an isotherm equation to relate the equilibrium concentration of the adsorbate in the solution and on GAC. The equation can be of any general form. A nonlinear isotherm of the form (Table 1) proposed by Redlich and Peterson (1959) has been

Table 1. Correlations for estimating model parameters

Parameters	Correlations	Data source/ref.
Isotherm	$q=\frac{aC}{1+bC^{\beta}}$ $a=15.1$, $b=7.55$, $\beta=0.8685$ at 25°C	Experiment (present work)
Fluidized-bed reactor voidage, ε	Richardson–Zaki equation	Yates (1983)
Liquid-phase axial dispersion coefficient, E_l	$\frac{E_l(X)}{\mu}=\frac{NR_e}{0.2+0.11N_{Re}^{0.48}}$	Chung and Wen (1968), Wen and Yu (1966)
Solid-phase axial dispersion coefficient, E_s	$E_s=0.04u^{1.8}$ m^2/s	Van Der Meer *et al.* (1984)
Film mass transfer coefficient, k_f	Correlated in terms of j-factor for packed and fluidized beds	Dwivedi *et al.* (1977)
Effective diffusivity	$De=4.1\times10^{-12}$ m^2/s at 25°C (#18/20 mesh GAC) $De=5.15\times10^{-12}$ m^2/s at 25°C (#12/14 mesh GAC)	Veeraraghavan *et al.* (1989)

adopted in this work. The equation can be generalized as

$$q_z(R, t)=f(C^*). \tag{4}$$

Equations (1)–(4) constitute a complete set of equations for simulating the adsorber performance. The equations have been expressed in the dimensionless form (see Appendix).

SIMULATION

This section presents an algorithm to simulate the fluidized-bed adsorber behavior as described by eqs (1)–(4). This is ensued by results of the numerical experiments to examine the model for parameter sensitivity and the numerical scheme for stability.

Algorithm

The computational procedure for simulating the fluidized-bed adsorber performance is outlined in Fig. 2. The adsorbate concentration profile within a GAC particle changes relatively slowly. Consequently, the equilibrium concentration at the GAC particle surface, α_z^*, is approximately constant over a small time period. To simplify the computational process, it is assumed that α_z^* remains constant during a small time step Δt when integrating the coupled PDES [eqs (1) and (2)]; this is the so-called pseudosteady-state assumption. The accuracy of the simulation can be improved by reducing the size of Δt continually. However, this process would cause the computational time to increase significantly. In the results presented in this paper (Figs 1–15), the step size is approximately one hundredth of each of the run completion time. This has been found to give convergence upto the second decimal point in the results. It needs to be pointed that more number of steps may be required as the column length is increased to achieve a similar degree of convergence.

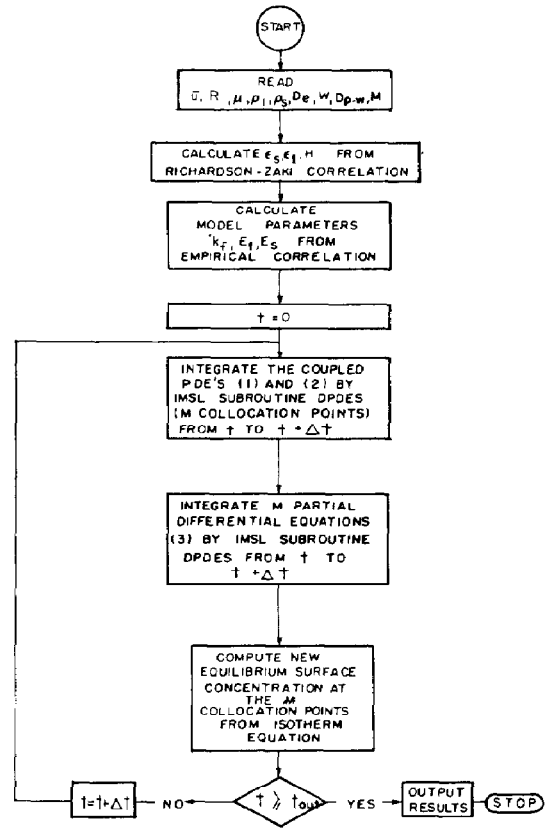

Fig. 2. Algorithm for simulating the fluidized-bed adsorber performance.

The adsorption isotherm and the effective diffusivity of phenol in GAC have been determined from independent experiments (Table 1). The rest of the model parameters have been estimated from available em-

pirical correlations. Thus, the model provides *a priori* means of predicting the adsorber performance.

Parameter sensitivity

Numerical experiments have been performed to assess the sensitivity of simulation results to the following model parameters:

(a) effective intraparticle diffusivity,
(b) external film mass transfer coefficient,
(c) solid-phase axial dispersion coefficient,
(d) liquid-phase axial dispersion coefficient.

In performing sensitivity analyses of the adsorber, it is important to choose parameter values in the normal operating range in order to understand the influence of the parameters on its performance. Hence, a typical laboratory-scale run condition has been chosen for the present study (Table 2). The parameter values at this condition have been determined based either on the independent experiments or available empirical correlations as outlined in Table 1. The variation of the effective diffusivity with particle size is probably caused by the fact that the arithmetic mean diameter used in the calculations is not the true characteristic

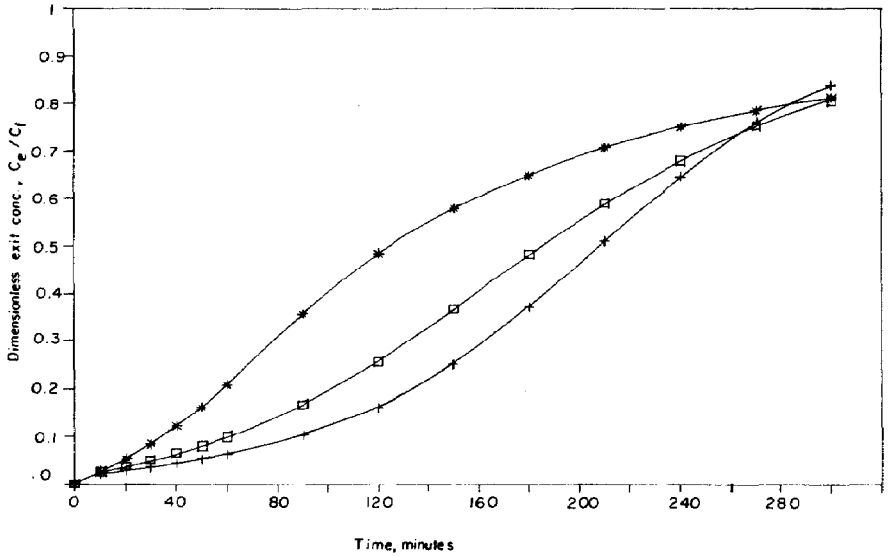

Fig. 3. Sensitivity analysis: effect of the intraparticle transport coefficient D_e on the breakthrough curve; *$0.3D_e$, □ $1.0D_e$, +$3.0D_e$.

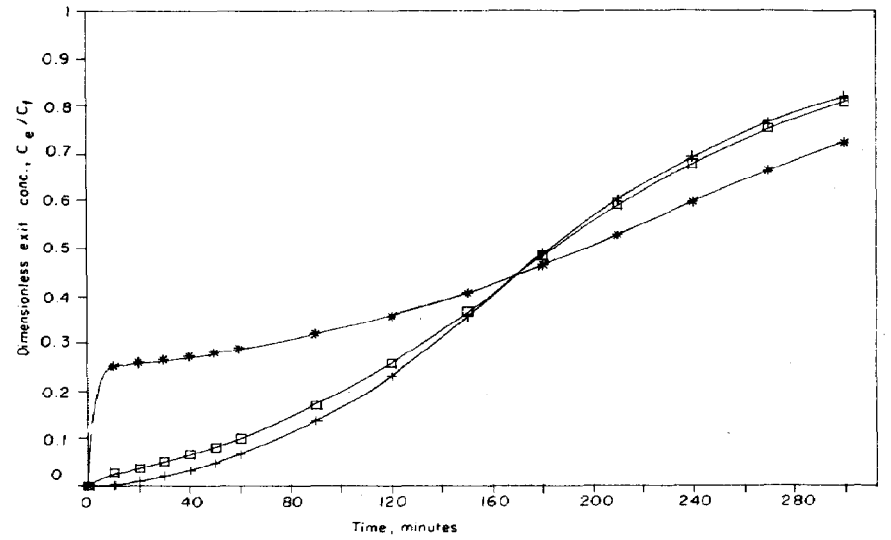

Fig. 4. Sensitivity analysis: effect of the external film mass transfer coefficient k_f on the breakthrough curve; * $0.3k_f$, □ $1.0k_f$, +$3.0k_f$.

Table 2. Run conditions employed in sensitivity analysis

Mean GAC particle size	9.2×10^{-4} m (#18/20 US mesh)
Amount of GAC	0.075 kg
Phenol solution feed concentration	1.41 mol/m^3
Feed solution flow rate	8×10^{-6} m^3/s (480.0 ml/min)

D_e, k_f, E_s and E_l were estimated as outlined in Table 1

dimension of the irregularly shaped adsorbent particles (Veeraraghavan *et al.*, 1989). The parameters in the isotherm equation have been estimated by the bottle point method with powdered activated carbon (Kunjupalu, 1986). The sensitivity analyses have been performed by perturbing each of the parameters while holding the rest of the conditions constant. The results are plotted in Figs 3–6.

It can be seen that the shape of the breakthrough curve is significantly influenced by the magnitude of the effective diffusivity (Fig. 3) and that of the external film mass transfer coefficient (Fig. 4). The initial stages of the breakthrough curves are very nearly identical for the three values of intraparticle effective diffusivity in Fig. 3. This indicates that the initial breakthrough profile is primarily a function of the external film mass transfer coefficient. The result is understandable since the effect of intraparticle diffusivity is negligible at the initial stage due to the large concentration gradient inside the particle. Perturbing the solid-phase mixing

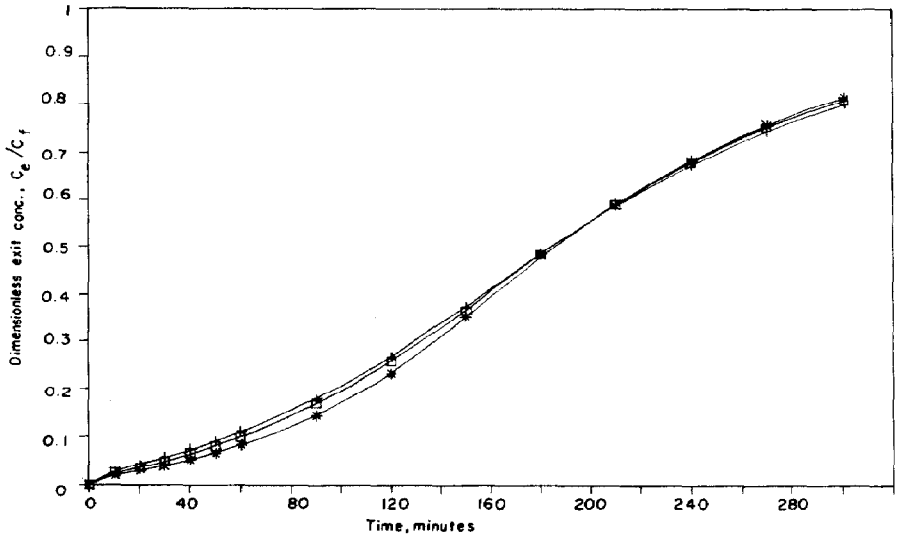

Fig. 5. Sensitivity analysis: effect of the solid-phase mixing coefficient E_s on the breakthrough curve; $+0.3E_s$, □ $1.0E_s$, * $3.0E_s$.

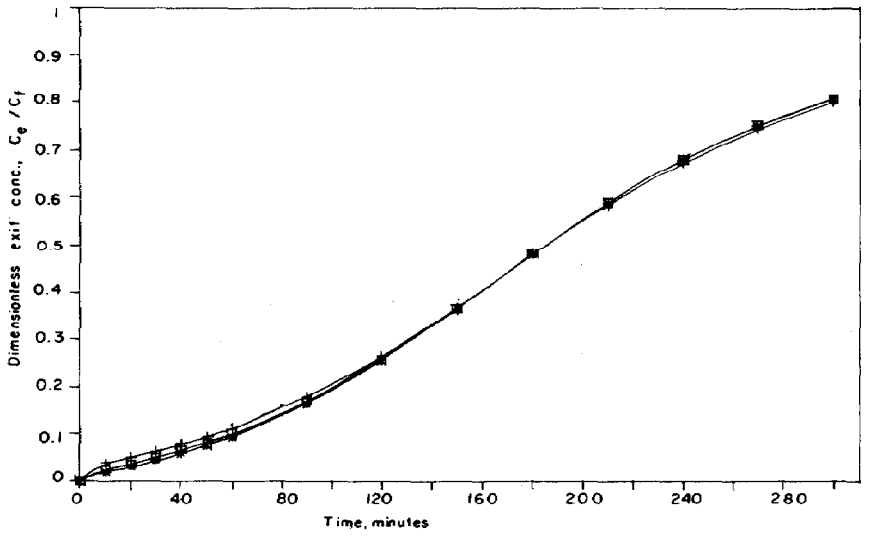

Fig. 6. Sensitivity analysis: effect of the liquid-phase axial dispersion coefficient E_l on the breakthrough curve; + 0.3 E_l, □ $1.0E_l$, * $3.0E_l$.

coefficient has only a slight effect on the breakthrough curve (Fig. 5). The effect of axial dispersion in the liquid-phase can be neglected in a packed bed when the ratio of bed height to particle diameter exceeds 50 (Carberry, 1976). This should approximately hold for liquid–solid fluidized beds since these beds can be viewed as expanded packed beds (Wen and Fan, 1975). In the present study, the ratio of bed height to particle diameter typically exceeds 500; hence, we expect negligible impact of liquid phase axial dispersion on adsorber performance. This has indeed been confirmed through simulations (Fig. 6).

It must be recognized that the above analysis is related to the experimental conditions employed in the present study. The model can be quite sensitive to the solid mixing and liquid-phase axial dispersion coefficient under an altered set of conditions. For instance, the model is sensitive to the solid-mixing parameter when the bed height is increased by a factor of 10 (Fig. 7) or when the phenol concentration in the feed solution is relatively low (in the order of 0.1 mol/m^3). The simulation results also indicate that large gradients in the adsorbate concentration on GAC can exist along the axial direction when employing a relatively long column. Similarly, the liquid-phase axial dispersion can be significant when employing very short columns. Such columns are, however, unlikely to be encountered in industrial practice.

Stability of the numerical scheme

The coupled set of parabolic partial differential equations, (1) and (2), have been integrated by calling the IMSL scientific library subroutine DPDES (Sewell, 1982). The algorithm is based on the method of orthogonal collocation on finite elements and employs cubic hermite polynomials as basis functions to expand the solution (Finlayson, 1980). It has been noticed that the numerical scheme becomes unstable when either the axial dispersion coefficients are made small or the bed length is increased by a large magnitude or, in other words, the PDEs take on an increasingly hyperbolic characteristic. For instance, in order to understand the influence of axial solid mixing on the performance of a long column (Fig. 7), we attempted simulation with the axial dispersion coefficient reduced by a factor of 3, but the scheme becomes unstable at these conditions. The problem can be circumvented to some extent by increasing the number of collocation points but this cannot be done indefinitely since we encounter other difficulties such as excessive computation time and numerical underflow errors. A suitable numerical scheme under these conditions will be the method of lines with upwind differencing of the convective flux terms (Smith, 1985) or the method of characteristics if the terms for axial mixing can be neglected (Khanna and Seinfeld, 1987; Lapidus and Pinder, 1982). These, however, are not the preferred methods when alternatives are available since the method of characteristics is extremely cumbersome to program and the finite difference scheme requires a relatively large number of mesh points and consequently, long computation times.

It is to be noted that the axial dispersion terms provide stability to the computation scheme. This by itself may justify retaining these terms even under conditions in which ignoring the terms will have negligible effect on model results.

EXPERIMENTAL VERIFICATION

In order to validate the present model, it has been fitted to experimental data obtained with a laboratory-scale adsorber for removing phenol from dilute

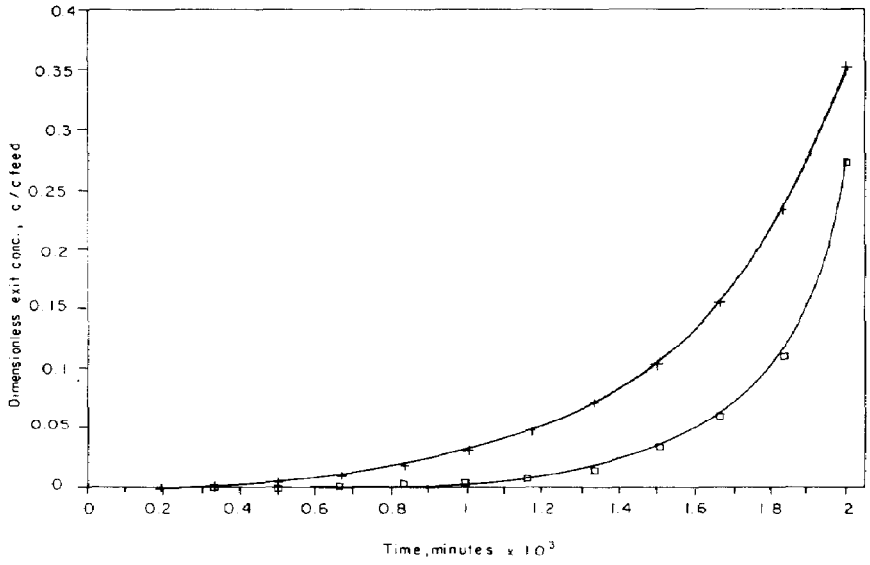

Fig. 7. Sensitivity analysis: effect of the solid-phase mixing coefficient E_s on the breakthrough curve in a relatively long column (GAC = 0.75 kg); + $3.0E_s$, □ $1.0E_s$.

solution. A description of the experiments and the results are given here.

Experiments

The adsorption experiments were conducted in a 2.54×10^{-2} m (1 in.) diameter glass column. The column was packed with 3.2×10^{-3} m ($\frac{1}{8}$ in.) glass beads at the inlet to distribute the liquid uniformly into the column. A schematic diagram of the experimental set-up is shown in Fig. 8. The adsorber was packed with GAC particles of a narrow size range at the outset of each run. The feed concentration, temperature, and flow rate of the phenol solution were maintained constant during the course of a run. The solution pH was initially adjusted to below 7.0 with 1.0 N sulfuric acid to convert phenol to its unionized form. The temperature was maintained at 25 ± 1°C.

The experimental conditions were chosen over a range of the solution flow rate, fluidized-bed height and GAC particle sizes. Specifically, the experiments were performed with two average GAC particle sizes viz. 9.2×10^{-4} m (#18/20 US mesh) and 1.545×10^{-3} m (#12/14 US mesh). Different solution flow rates have been applied at each of the particle sizes. Tests have also been conducted with varying amounts of carbon with #12/14 mesh GAC. Under the conditions tested, particulate fluidization was observed. No elutriation of GAC particles was inherent in the runs. The breakthrough profiles were determined by monitoring spectrophotometrically the concentration of phenol in the exit solution.

Results

The experimentally observed concentration of phenol in the exit solution is compared with model prediction in Figs 9–15. The results of simulation and

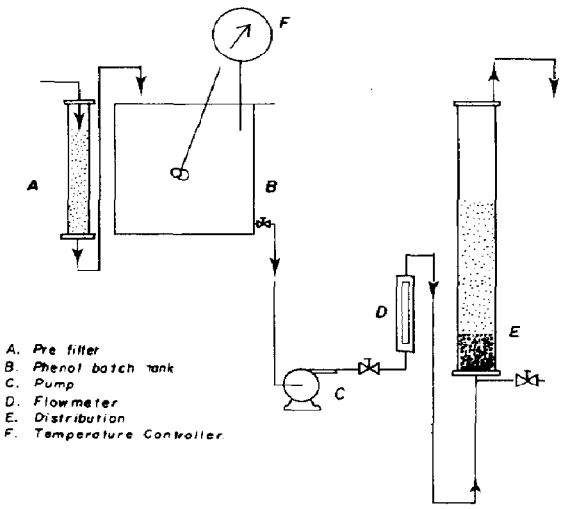

Fig. 8. Schematic of the experimental set-up.

experiment are in good agreement for the early part of breakthrough curve. Some of the runs have been repeated to test for consistency of experimental results (see Figs 9–11). In the duplicate runs, the simulations have been performed at the average conditions as there are small differences among the experimental conditions. As can be seen, the effect on breakthrough profile due to these differences are very slight.

DISCUSSION

As indicated in the preceding section, agreement between the experiments and model is in general excellent in the early segment of the breakthrough curve (Figs 9–15); however, the predicted breakthrough concentrations are significantly lower than

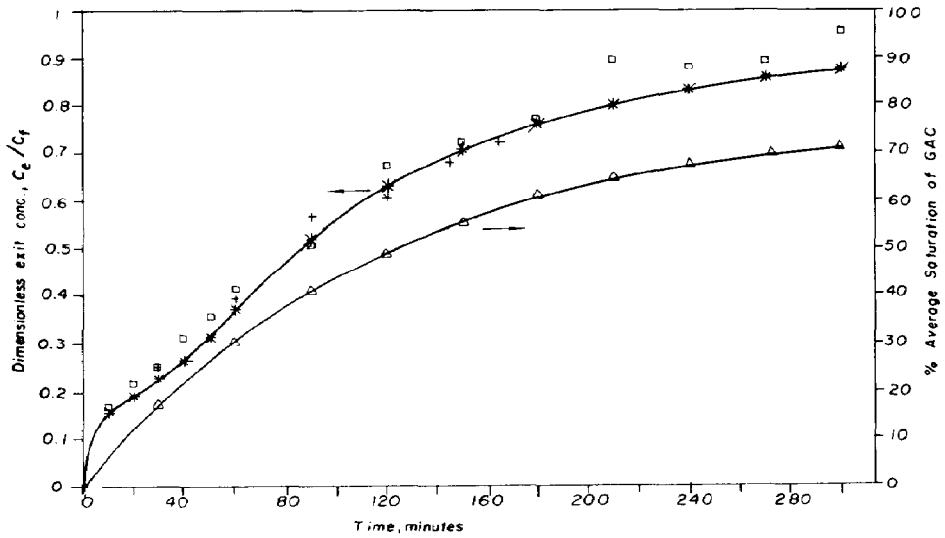

Fig. 9. Fluidized-bed adsorber breakthrough curve with 0.075 kg of 1.545×10^{-3} m ϕ (# 12/14 mesh) GAC: □ experiment with $C_f = 2.02$ mol/m^3, $\bar{u} = 0.0181$ m/s; + experiment with $C_f = 1.88$ mol/m^3, $\bar{u} = 0.0174$ m/s; — * — simulation with $C_f = 1.95$ mol/m^3, $\bar{u} = 0.0178$ m/s.

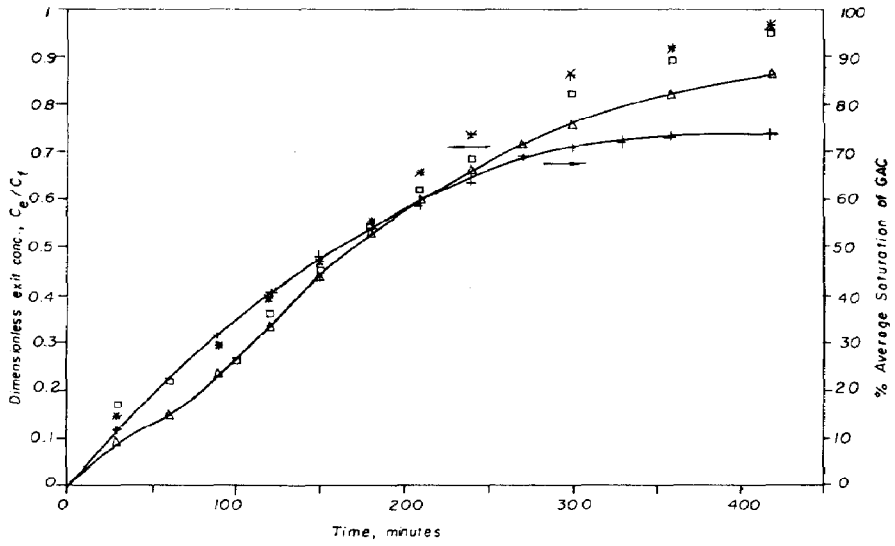

Fig. 10. Fluidized-bed adsorber breakthrough curve with 0.08 kg of 1.545×10^{-3} m ϕ (# 12/14 mesh) GAC: * experiment with $C_f = 1.93$ mol/m^3, $\bar{u} = 0.0122$ m/s; □ experiment with $C_f = 1.95$ mol/m^3, $\bar{u} = 0.0115$ m/s; —△— simulation with $C_f = 1.94$ mol/m^3, $\bar{u} = 0.0118$ m/s.

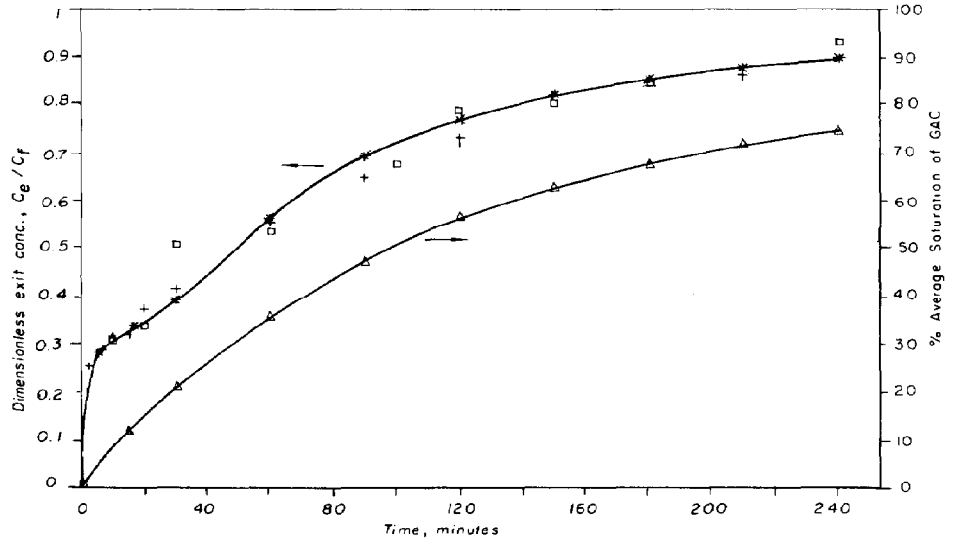

Fig. 11. Fluidized-bed adsorber breakthrough curve with 0.04 kg of 1.545×10^{-3} m ϕ (# 12/14 mesh) GAC: + experiment with $C_f = 2.03$ mol/m^3, $\bar{u} = 0.0132$ m/s; □ experiment with $C_f = 2.01$ mol/m^3, $\bar{u} = 0.0135$ m/s; — * — simulation with $C_f = 2.02$ mol/m^3, $\bar{u} = 0.133$ m/s.

experimental values towards the end. The difference between the model predictions and experimental results widens as the average saturation of the GAC increases approximately beyond 70% of the equilibrium or maximum loading. This is probably due to the inhomogeneous pore structure in GAC. To overcome this difficulty, Seidel and Gelbin (1986) have modeled the GAC as having two pore zones with different adsorption capacities and different diffusivities. In applying the two-zone model, Reschke *et al.* (1986) have found that rapid adsorption occurs in the micropores containing 70–80% of the adsorption capacity which is followed by slow adsorption. Nevertheless, the values of the effective diffusivity used in the present simulations have been obtained from batch kinetic experiments by assuming that the effective diffusivity is constant and that the homogeneous solid diffusion model is applicable. Also, in determining the model parameters from the batch data, curve fitting was carried out for data up to approximately 70% saturation of GAC (Veeraraghavan *et al.*, 1989). Therefore, the diffusivity value used is probably high for the final stage of adsorption. This, in turn, can cause the observed discrepancy between the exper-

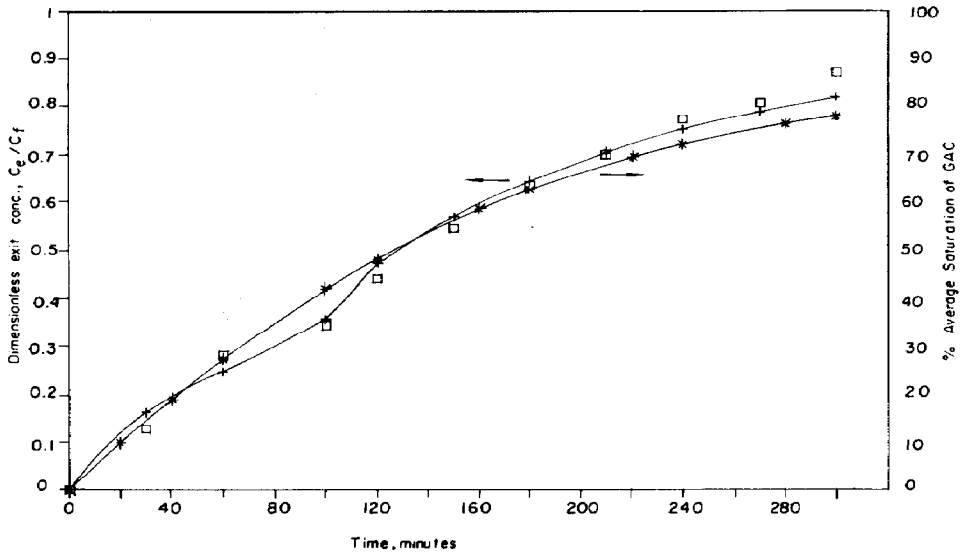

Fig. 12. Fluidized-bed adsorber breakthrough curve with 0.06 kg of 1.545×10^{-3} m ϕ (# 12/14 mesh) GAC: □ experiment with $C_f = 1.82$ mol/m^3, $\bar{u} = 0.0115$ m/s; —+— simulation with $C_f = 1.82$ mol/m^3, $\bar{u} = 0.0115$ m/s.

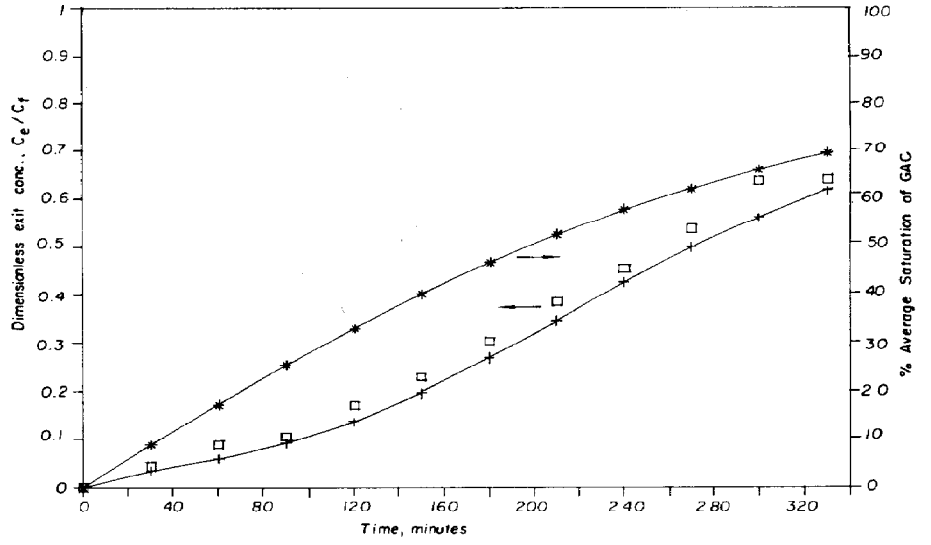

Fig. 13. Fluidized-bed adsorber breakthrough curve with 0.075 kg of 1.545×10^{-3} m ϕ (# 12/14 mesh) GAC: □ experiment with $C_f = 2.02$ mol/m^3, $\bar{u} = 0.0075$ m/s; —+— simulation with $C_f = 2.02$ mol/m^3, $\bar{u} = 0.0075$ m/s.

imental and simulated results. It is expected that the model can be further refined by incorporating into it the slow-down in the intraparticle transport observed in the experiments.

The difference between experimental and simulated results toward the end of the runs is particularly pronounced for # 18/20 mesh GAC. This again can be understood on the basis of the observed slow-down in intraparticle transport. It should be noted that the experiments with 9.2×10^{-4} m diameter (# 18/20 mesh) GAC have been carried out 2 to 3 times longer that the experiments with 1.545×10^{-3} m diameter (# 12/14 mesh) GAC in terms of the dimensionless time, R^2/D_e based on the intraparticle diffusivity. At such relatively long times, the effect of slow down in the transport rate is highly pronounced. This effect is also observed in the run which has been carried out for the longest length of time with # 12/14 mesh carbon (Fig. 10).

It is worth noting that the experiments were performed under conditions in which the results were not sensitive to small changes in the values of the solid and liquid phase dispersion coefficients. Hence, it is not possible to judge the suitability of the correlations for

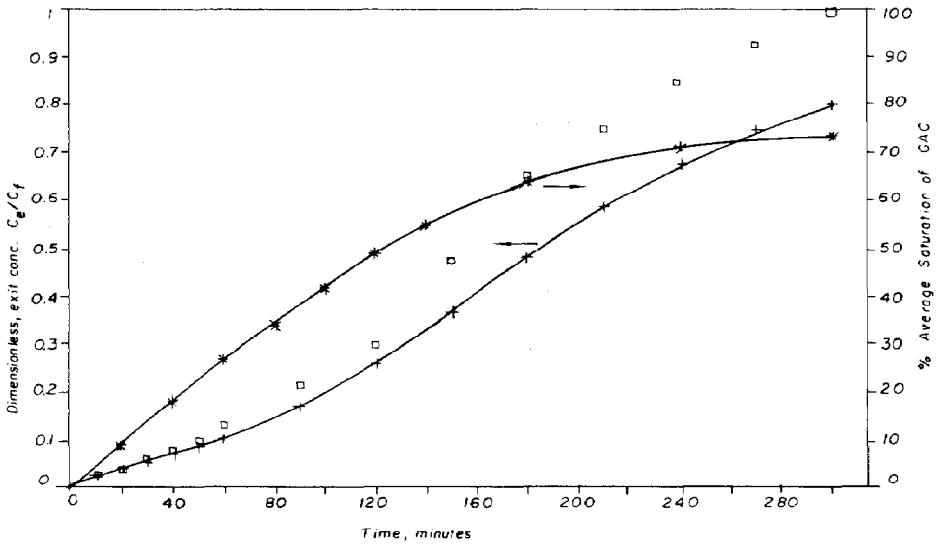

Fig. 14. Fluidized-bed adsorber breakthrough curve with 0.075 kg of 0.92×10^{-3} m ϕ (# 18/20 mesh) GAC: □ experiment with $C_f = 1.41$ mol/m^3, $\bar{u} = 0.0157$ m/s; —+— simulation with $C_f = 1.41$ mol/m^3, $\bar{u} = 0.0157$ m/s.

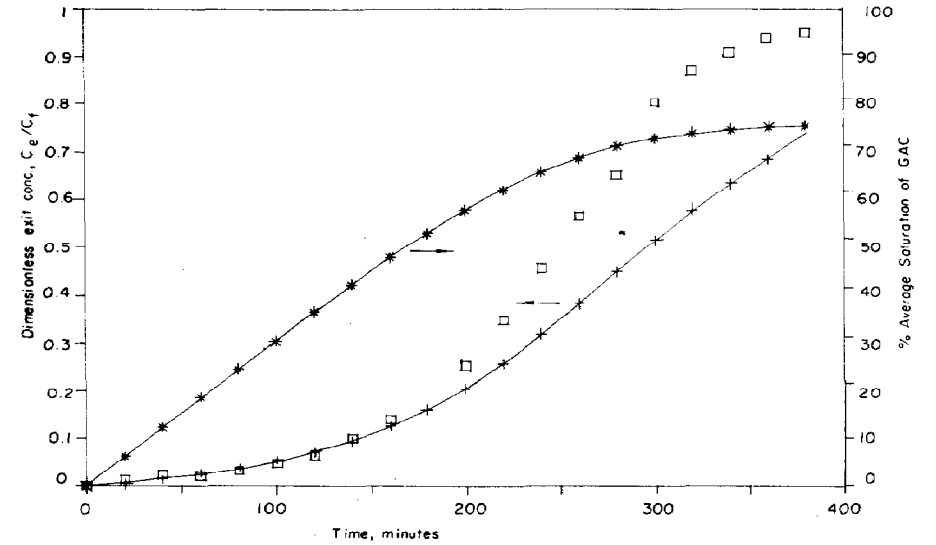

Fig. 15. Fluidized-bed adsorber breakthrough curve with 0.075 kg of 0.92×10^{-3} m ϕ (# 18/20 mesh) GAC: □ experiment with $C_f = 1.88$ mol/m^3, $\bar{u} = 0.0083$ m/s; —+— simulation with $C_f = 1.88$ mol/m^3, $\bar{u} = 0.0083$ m/s.

axial dispersion coefficients in a priori modeling (Table 1). On the other hand, since most practical columns will be relatively long and since fluidization requires a certain minimum liquid flow velocity, it is to be expected that the liquid-phase axial dispersion will have only a minor impact on the system performance. It should be adequate to physically model the liquid-phase flow behavior as plug flow.

CONCLUDING REMARKS

A dynamic mathematical model incorporating the dominant mechanistic features has been developed to describe the removal of phenol from aqueous solution in a fluidized-bed adsorber with GAC. It has been shown that the breakthrough profile can be sensitive to solid mixing parameter in a relatively deep adsorption bed; hence, it is vital to have a good understanding of the solid mixing phenomenon. On the other hand, the liquid-phase flow behavior can be safely modeled as plug flow. Nevertheless, it is to our advantage to include the liquid-phase axial dispersion as this requires only a small amount of extra computational effort and pays off handsomely in the form of enhanced numerical stability [also see Khanna and Seinfeld (1987)]. The simulated results compare well

with the experimental results obtained from a bench-scale fluidized-bed adsorber, particularly in the early stages of the batch experiments. The probable reason for the difference between the experiment and model in the later stage of a run has been identified.

Acknowledgements—We are grateful to the National Science Foundation for financial assistance (Grant No. ECE 8507422) in carrying out this research. The numerical computations for this research were carried out using the Cornell National Supercomputer Facility, a resource of the Center for Theory and Simulation in Science and Engineering at Cornell University, which is funded in part by the National Science Foundation, New York State, and the IBM Corporation and members of the Corporate Research Institute.

NOTATION

Bi Biot number, $k_f R/D_e$
C concentration of the adsorbate in the liquid phase, mol/m^3
C^* local equilibrium concentration in the liquid phase corresponding to the adsorbate concentration at the GAC particle boundary, mol/m^3
C_e exit solution concentration, mol/m^3
C_f solution feed concentration, mol/m^3
D_e effective diffusivity of the adsorbate into the GAC particle, m^2/s
D_{p-w} diffusivity of phenol in water at 25°C, m^2/s
E_l axial liquid-phase dispersion coefficient, m^2/s
E_s axial solid-phase dispersion coefficient, m^2/s
H height of adsorber, m
k_f liquid-phase mass transfer coefficient, m/s
Pe liquid-phase axial Peclet number, $\bar{u}H/\varepsilon_1 E_1$
q adsorbate concentration in the GAC particle, mol/kg
q_{max} equilibrium concentration in the GAC particle according to eq. (4) corresponding to the feed concentration of the solution, mol/kg
R GAC particle radius, m
r radial position in the GAC particle, m
t time, s
$\bar{u}$ superficial fluid velocity, m/s
W amount of GAC in column, kg

Subscripts
l liquid phase
s solid phase

Greek letters
α dimensionless adsorbate concentration in the liquid phase, C/C_f
α^* dimensionless equilibrium liquid-phase concentration at the GAC particle surface, C^*/C_f
β dimensionless adsorbate concentration in the GAC particle, q/q_{max}
$\bar{\beta}$ volumetric average adsorbate concentration in the GAC particle, $\bar{q}/q_{max}$
ϕ arithmetic mean of the mesh sizes passing and retaining the GAC particles, m
ε_s volume fraction of the solid phase
ε_l volume fraction of the liquid phase
η dimensionless radial position in the GAC particle, r/R
μ solution viscosity, kg/m s
ρ_p apparent density of GAC particle, kg/m^3
Θ dimensionless time, t/τ
θ_r dimensionless residence time, $H\varepsilon_1/\bar{u}\tau$
τ characteristic time R^2/D_e, s
ζ dimensionless height, z/H

REFERENCES

Carberry, J. J., 1976, *Chemical and Catalytic Reaction Engineering*, pp. 156–159; 532–537. McGraw-Hill, New York.

Carlos, C. R. and Richardson, J. F., 1968, Solids movements in liquid fluidized beds—I. Particle velocity distribution. *Chem. Engng Sci.* **23**, 813–824.

Chung, S. F. and Wen, C. Y., 1968, Longitudinal dispersion of liquid flowing through fixed and fluidized beds. *A.I.Ch.E. J.* **14**, 857–866.

Culp, R. L., Wesner, G. M. and Culp, G. L., 1978, *Handbook of Advanced Wastewater Treatment*, pp. 166–245. Van Nostrand Reinhold, New York.

Dwivedi, P. N. and Upadhyay, S. N., 1977, Particle–fluid mass transfer in fixed and fluidized beds. *Ind. Engng Chem. Process Des. Dev.* **16**, 157–165.

Finlayson, B. A., 1980, *Nonlinear Analysis in Chemical Engineering*, pp. 113–126. McGraw-Hill, New York.

Khanna, R. and Seinfeld, J. S., 1987, *Advances in Chemical Engineering*, pp. 113–191. Academic Press, New York.

Kunjupalu, T., 1986, Effect of particle size distribution on activated carbon adsorption. M.S. Thesis, Kansas State University, Manhattan.

Lapidus, L. and Pinder, G. F., 1982, *Numerical Solution of Partial Differential Equations in Science and Engineering*, pp. 21–33. John Wiley, New York.

Mathews, A. P. and Fan, L. T., 1983, Comparison of performance of packed and semifluidized beds for adsorption of trace organics. In *Adsorption and Ion Exchange*—83, *A.I.Ch.E. Symp. Ser.* No. 230, **79**, 79–85.

Potter, O. E., 1971, Mixing in *Fluidization* (Edited by J. F. Davidson, and D. Harrison), pp. 293–381. Academic Press, New York.

Redlich, O. and Peterson, D. L., 1959, A useful adsorption isotherm. *J. Phys. Chem.* **63**, 1024.

Reschke, G., Radeke, K. H. and Gelbin, D., 1986, Breakthrough curves for single solutes in beds of activated carbon with broad pore size distribution—II. Measuring and calculating breakthrough curves of phenol and indole from aqueous solutions on activated carbons. *Chem. Engng Sci.* **41**, 549–554.

Ruthven, M. D., 1984, *Principles of Adsorption and Adsorption Process*, pp. 166–205. John Wiley, New York.

Sewell, G., 1982, IMSL software for differential equations in one space variable, IMSL Technical Report Series 8202, January 1982.

Seidel, A. and Gelbin, D., 1986, Breakthrough curves for single solutes in bed of activated carbon with a broad pore size distribution—I. Mathematical models of breakthrough curves in beds of activated carbon. *Chem. Engng Sci.* **41**, 541–548.

Smith, G. D., 1985, *Numerical Solution of Partial Differential Equations: Finite Difference Methods*, pp. 175–220. Oxford University Press, New York.

Suzuki, M. and Kawazoe, K., 1975, Effective surface diffusion coefficients of volatile organics on activated carbon during adsorption from aqueous solution. *J. Chem. Engng Japan* **8**, 379–382.

Van Der Meer, A. P., Blanchard, C. M. R. J. P. and Wesselingh, J. A., 1984, Mixing of particles in liquid fluidized beds. *Chem. Engng Res. Des.* **62**, 214–222.

Veeraraghavan, S., Mathews, A. P. and Fan, L. T., 1989, Effects of solute concentration and geometric characteristics of particles on intraparticle diffusivity and adsorber dynamics. Paper presented at the *Third Int. Conf. on Fundamentals of Adsorption*, Nurtingen, F.R.G., 7–12 May 1989.

Wen, C. Y. and Fan, L. T., 1975, *Models for Flow Systems and Chemical Reactors*, pp. 150–166. Marcel Dekker, New York.

Wen, C. Y. and Yu, Y. H., 1966, A generalized method for predicting the minimum fluidization velocity. *A.I.Ch.E. J.* **12**, 610–612.

Yates, J. G., 1983, *Fundamentals of Fluidized-bed Chemical Processes*, pp. 9–15. Butterworths, Kent, U.K.

APPENDIX: SYSTEM EQUATIONS IN DIMENSIONLESS FORM

The intraparticle transport coefficient, D_e, is the single most important parameter in determining the shape of the breakthrough curve. Hence, the characteristic time for the system is taken as

$$\tau = \frac{R^2}{D_e}. \tag{A-1}$$

Equations (1)–(4) in the text can then be written in the dimensionless form as follows.

(a) The liquid-phase continuity equation [eq. (1) in text].

$$\theta_r \frac{\partial \alpha}{\partial \theta} = \frac{1}{Pe}\frac{\partial^2 \alpha}{\partial \zeta^2} - \frac{\partial \alpha}{\partial \zeta} - 3Bi\theta_r \frac{\varepsilon_s}{\varepsilon_1}(\alpha - \alpha^*). \tag{A-2}$$

The initial and boundary conditions are

$$\theta = 0, \quad \alpha(0, \zeta) = \alpha_\zeta(0), \quad 0 \leqslant \zeta \leqslant 1 \tag{A-2a}$$

$$\zeta = 0, \quad \alpha - \frac{1}{Pe}\frac{\partial \alpha}{\partial \zeta} = 1, \quad \theta > 0 \tag{A-2b}$$

$$\zeta = 1, \quad \frac{\partial \alpha}{\partial \zeta} = 0, \quad \theta > 0. \tag{A-2c}$$

(b) The solid-phase continuity equation [eq. (2) in text].

$$\varepsilon_s \frac{\partial \bar{\beta}}{\partial \theta} = \frac{E_s \tau}{H^2}\frac{\partial^2 \bar{\beta}}{\partial \zeta^2} + 3Bi \cdot \frac{C_f}{\rho_p q_{max}} \varepsilon_s(\alpha - \alpha^*). \tag{A-3}$$

The initial and boundary conditions are

$$\theta = 0, \quad \bar{\beta}(0, \zeta) = \bar{\beta}_\zeta(0), \quad 0 \leqslant \zeta \leqslant 1 \tag{A-3a}$$

$$\zeta = 0, \quad \frac{\partial \bar{\beta}}{\partial \zeta} = 0, \quad \theta > 0 \tag{A-3b}$$

$$\zeta = 1, \quad \frac{\partial \bar{\beta}}{\partial \zeta} = 0, \quad \theta > 0. \tag{A-3c}$$

(c) The continuity equation for GAC particle at position ζ [eq. (3) in text].

$$\frac{\partial \beta_\zeta}{\partial \theta} = \frac{1}{\eta^2}\frac{\partial}{\partial \eta}\left[\eta^2 \frac{\partial \beta_\zeta}{\partial \eta}\right]. \tag{A-4}$$

The initial and boundary conditions are

$$\theta = 0, \quad \beta_\zeta(\eta, 0) = \beta(\zeta, \eta, 0), \quad 0 \leqslant \eta \leqslant 1 \tag{A-4a}$$

$$\eta = 0, \quad \frac{\partial \beta_\zeta}{\partial \eta} = 0, \quad \theta > 0 \tag{A-4b}$$

$$\eta = 1, \quad \frac{\partial \beta_\zeta}{\partial \eta} = -\frac{1}{3}\frac{\partial \bar{\beta}_\zeta}{\partial \theta}, \quad \theta > 0. \tag{A-4c}$$

(d) The isotherm equation [eq. (4) in text].

$$\beta(1, \Theta) = g(\alpha^*, C_f). \tag{A-5}$$